**Canadian Conference - Pacific Conference on Earthquake Engineering 2023**

**Vancouver, British Columbia**

**June 25th – June 30th, 2023**


# Vulnerability Assessment of Coastal Bridges Subjected to Tsunami Loading

Jesika Rahman[1] and AHM Muntasir Billah[2*]

[1]PhD Student, Department of Civil Engineering, University of Calgary, Calgary, AB, Canada
[2]Assistant Professor, Department of Civil Engineering, University of Calgary, Calgary, AB, Canada
[*]muntasir.billah@ucalgary.ca (Corresponding Author)

## ABSTRACT

The consequences of tsunamis often lead to severe damage to coastal bridges, resulting in socioeconomic loss, delays in rescue operations and even loss of human lives. It is therefore important to quantify the vulnerability to improve the resiliency of coastal bridges subjected to tsunami loading with the use of risk-informed decision-making tools. This study aims to present the vulnerability assessment of the bearings and piers of coastal bridges subjected to tsunami loads. Numerical simulation of loads due to tsunami is carried out which includes the hydrostatic, hydrodynamic and debris load components. Numerical finite element models of the selected prototype reinforced concrete I-girder coastal bridge located in Vancouver Island, BC, are developed in OpenSees. Based on the flow depth and flow speed of water and the corresponding wave period and wave height as intensity measures, three load cases are analyzed namely loads due to maximum flow speed with reduced flow depth, maximum flow depth with reduced flow speed and large water-borne debris with reduced flow speed and flow depth, respectively. The loads are applied to the bridge deck as well as the piers in both vertical and horizontal directions. The vulnerability of the elastomeric bearing and circular piers is determined by comparing the maximum deformation of the components with the damage states developed for the bearings and circular piers of coastal bridge systems subjected to extreme wave loads. The analysis revealed that even though the flow speed and depth were the least out of the three cases, the piers and bearings experienced the most damage due to case 3 loading due to the effect of debris loads. The elastomeric bearings are found to be the most vulnerable component due to the loading cases considered. The outcomes of this paper could aid in the fragility analysis of coastal structures exposed to tsunamis.

Keywords: Tsunami load calculations, Coastal bridge, OpenSees, Elastomeric bearing and Vulnerability assessment.

## INTRODUCTION

Coastal bridges are lifeline structures that connect the affected regions to safety during extreme hazard events like a tsunami. Tsunami events mostly originate from the large sudden displacements of the earth's surface in an offshore region during earthquakes causing a large displacement of water in the ocean. The coastal infrastructures faced catastrophic consequences during the Indian Ocean tsunami in 2004, Chile tsunami in 2010 and the Tohoku tsunami in 2011 [1, 2]. Therefore, a growing number of studies are being carried out to understand the failure mechanism of coastal bridges under the action of a tsunami.

Azadbakht and Yim [3] investigated tsunami wave load on coastal girder bridge decks by dividing their study into two stages, one signifying the event when tsunami water surface elevation reached the bottom chord of the deck and then overtopping the deck. The other stage represented a situation when full inundation of the entire bridge occurred. The vertical and horizontal forces and overturning moment acting on the bridge superstructure were calculated using finite element (FE) analysis in LS-DYNA. In a recent study by Feng et al. [4], the dynamic performance of a simply supported girder bridge subjected to the earthquake-tsunami cascading effect was analyzed. They modeled the prototype bridge in OpenSees and applied the earthquake loads followed by the simulated tsunami load time history. They identified that the bridge responses increased as the wave height of the sequential tsunami loads increased. The laminated rubber bearings were observed to withstand more damage in the longitudinal direction than that in the transverse direction. A few studies have been done in the past that analyzed the dynamic nature of bridge responses and fragility of coastal bridges due to action of wave-induced forces arising from extreme events like tsunami. Such is the study by Rahman and Billah [5] where the elastomeric bearing elements were found to the most vulnerable due to extreme wave loads. Studies by Qeshta [6] and Qeshta et al [7] also analyzed the vulnerability of coastal bridges due to extreme wave-induced forces and proposed retrofitting techniques using FRP strengthening of the bridge piers.

Although these studies have made remarkable progress in evaluating the failure mechanism and vulnerability assessments, the dynamic nature of the tsunami loads including the debris impact loads are yet to be analyzed.

Moreover, no practical design guidelines are available that can accurately represent the dynamic nature of the tsunami waves and debris impact loads. The Canadian Highway Bridge Design Code (CHBDC) [8] has specified the calculation of breaking wave forces to be included in the total water loads on structures which is a hydrostatic load having a constant flow speed. The Federal Highway Administration (FHWA) of the US Department of Transportation [9] published a report where a method of estimating wave loads on bridge decks using a modified version of the method by Douglas et al. [10] is presented. This method is heavily dependent on the geometry of the bridge deck and is it is recommended that it be used for the cases when the storm surge elevation is approximately close to the elevation of the bridge deck. To this end, this paper aims to investigate the dynamic effect of tsunami loads on coastal bridges by means of numerical analysis. The time histories of three typical tsunami load cases are generated following the linear wave theory and applied to the numerical FE model of the bridge in two scenarios. The response time histories from the bridge components (piers and elastomeric bearings) are then compared with the DSs defined earlier for coastal bridges subjected to extreme wave-induced loads. This paper is unique in the sense that it includes the effect of debris impact along with the total wave load time history.

## METHODOLOGY

The case study bridge selected is a three-span reinforced concrete (RC) I-girder bridge located in Vancouver Island, BC. This study is divided into two conditions, scenario 1 presents the event when tsunami water elevation do not inundate the piers completely and scenario 2 presents the complete inundation of the piers due to tsunami water elevation and the wave reach the superstructure. An illustration of the two scenarios can be found in Figure 1. 20 FE models of the bridge, where the material properties in piers are varied, are developed in the OpenSees software [11]. Three loading cases in each scenario are considered for analysis according to the report by Lynett et al. [12] as shown in Table 1. The first case represents maximum flow speed with reduced flow depth, case 2 represents maximum flow depth with reduced flow speed and case 3 presents reduced flow depth and flow speed with large water-borne debris load The wave parameters are chosen from typical extreme wave loading events recorded from the past [13]. The maximum value of the flow speed ($u_{max}$) is calculated based on the value of wave period ($T_w$) and the maximum value of flow depth ($\eta_{max}$) is calculated based on the corresponding value of maximum wave height ($H_w$). As tsunami events with maximum flow depth and flow speed are not likely, also large water borne debris flow occurring with maximum flow speed and depth are unlikely, separate cases for these events are considered [12]. Each of the 20 bridge models are applied with the three load cases under two scenarios giving a total of 120 simulation results to be post-processed and analyzed using MATLAB. In a coastal bridge system, when the bearing fails no connection exists between the superstructure and substructure thereby causing wash-out of the bridge deck. Moreover, piers are deemed to be one of the most critical component and can cause catastrophic failure of the bridge when it experiences severe damages. Therefore, the vulnerability assessment in this study is done considering pier drift and shear deformation of the elastomeric bearings as the engineering demand parameters (EDP). The maximum pier drift ratio and bearing deformation are compared with the damage states developed earlier [5] in order to assess the vulnerability of the piers and the elastomeric bearing. Tsunamis are generally classified as far-field when the point of origin of the earthquake is far away from the location of the structure being analyzed whereas the near-field tsunami occurs when the earthquake is close to the structure. In the case of far-field tsunamis, the effect of earthquake does not have a direct impact on the structure. This study considers only the far-field tsunami loads, so the direct effect of the cascading earthquake-tsunami loads is neglected.

*Table 1. Summary of tsunami load cases considered and the corresponding wave parameters*

| Load Case | Flow Speed | Corresponding wave period, $T_w$ | Flow Depth | Corresponding wave height, $H_w$ | Debris Load |
|---|---|---|---|---|---|
| 1 | $u_{max}$ | 3.37sec | 2/3 $\eta_{max}$ | 4.67m | -- |
| 2 | $0.8u_{max}$ | 4.04sec | $\eta_{max}$ | 7.00m | -- |
| 3 | $0.5u_{max}$ | 5.06sec | $0.5\eta_{max}$ | 3.15m | $F_{db}$ |

## BRIDGE DESCRIPTION AND FINITE ELEMENT MODEL

The general configuration of the bridge is shown in Figure 1 where the mid and end span lengths are 40m and 33m, respectively. The superstructure is supported at the end with the help of the abutments and by two intermediate double column RC bents in the middle. The piers have a diameter of 1.5m and are 11.5m and 16.5m high. The elastomeric bearing elements used to help transfer the load from superstructure to the piers have a dimension of 425×600×116 mm. The 3D nonlinear FE modeling of the bridge is done in OpenSees where the components of bridge are modeled as line elements that has 3D behavior to be used in the domain. The piers are modeled as displacement-based nonlinear beam-column elements using fiber section and the girders along with deck are modeled as elastic elements as per the assumption of their elasticity during the wave load interaction. The RC material is modeled using Concrete07, whereas Steel02 is used to model the reinforcement steel. The elastomeric bearings

are modeled using Steel01 in the transverse direction whereas the shear keys are modeled using the Hysteretic material, all of which are available in the OpenSees material library. Each of the bridge models has a different reinforcement ratio, concrete compressive strength and steel yield strength values in the piers while keeping the basic geometry of the entire bridge as it is. Details of the FE modeling technique and its validation can be found in [5]. The uncertainties considered in modeling the bridges are shown in Table 2 and the parameter considered for each bridge model can also be found in [5].

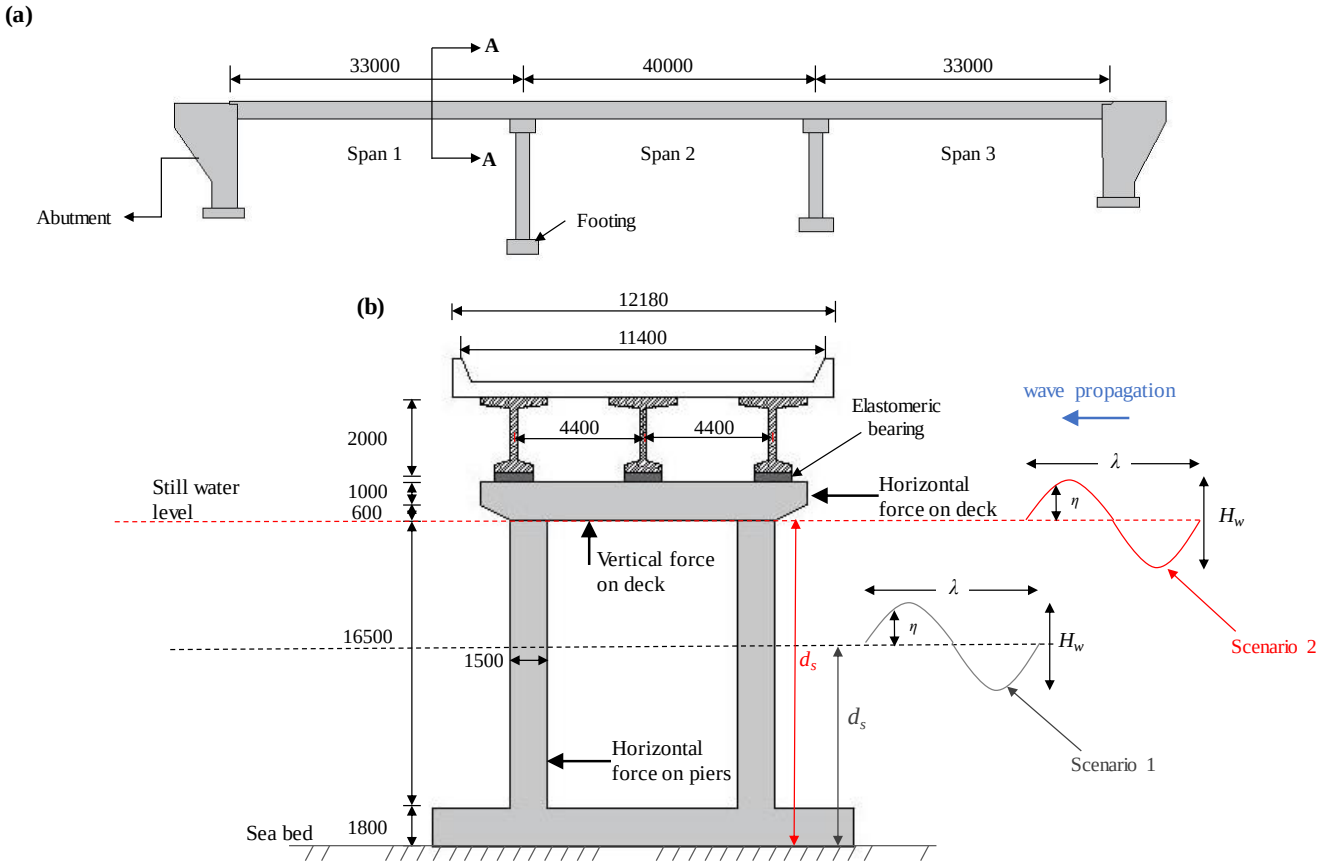


*Figure 1. General configuration of the case study bridge showing (a) the elevation view, and (b) the section A-A view showing scenarios 1 and 2 (all dimensions are in mm)*

*Table 2. Parameter uncertainties considered in bridge modeling*

| Parameter | Distribution | *Distribution Characteristics | | Unit | Reference |
|---|---|---|---|---|---|
| Concrete Compression, ($f_c$') | Normal | $\mu$ =30 | $\sigma$ = 4.30 | MPa | [14] |
| Steel Yield Strength ($f_y$) | Lognormal | $\lambda$ = 6.13 | $\xi$ = 0.08 | MPa | [14, 15] |
| Reinforcement Ratio ($\rho_s$) | Uniform | a = 1.12 | b = 1.50 | % | -- |

*Note: a = upper limit, b = lower limit, $\mu$ = mean of normal distribution, $\lambda$ = mean of lognormal distribution, $\sigma$ = standard deviation of normal distribution and $\xi$ = standard deviation of lognormal distribution.

## TSUNAMI LOADING CALCULATION

The factors responsible for tsunami loading intensity on coastal bridges are not limited to flow depth and flow speed, but also the debris flow and bridge geometry. The basic approach to calculating the tsunami loads in this study is to determine the time history of water particle motion and apply them to the corresponding components of wave and debris loads. The total horizontal wave loads include the horizontal component of drag, inertia, slamming and debris load whereas the vertical load includes the vertical components from drag, inertia, slamming (all three are acting downwards) and buoyancy forces (acting upwards). The time history of wave particle motion is calculated following the method described in [5] and the CHBDC [8] guideline is followed to determine the total wave force time history. More details on the calculation and validation of this method of wave load estimation are described in [5]. Figure 2 shows the calculated total horizontal force time history under cases 1 and 2.

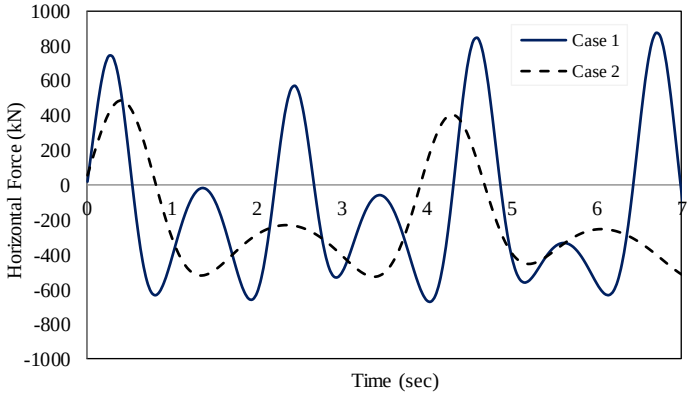


*Figure 2. Time history of case 1 and case 2 horizontal tsunami force on bridge deck*

According to Lynett et al. [12], the large water-borne debris including vehicles or shipping containers can cause a large horizontal impact force on coastal bridges. The flexible debris impact force ($F_{db}$) is calculated following the FEMA [16] guideline as shown in Eq. (1) where $u$ is the flow speed carrying the debris, $k$ is the effective stiffness coefficient, $m$ and $c$ denote the mass and the hydrodynamic mass coefficient of the debris, respectively. The effective stiffness coefficient as 43kN/mm, a mass of 1100kg representing a typical shipping container and the hydrodynamic coefficient as zero are considered for the debris flow in this study following the recommendations by Naito et al. [17]. 1.3 in the equation is due to the importance factor accounting for critical infrastructure. In this study, a time history of the debris force is obtained as the time history of the water article carrying the debris is generated as shown in Figure 3.

$$F_{db}=1.3u\sqrt{km(1+c)} \tag{1}$$

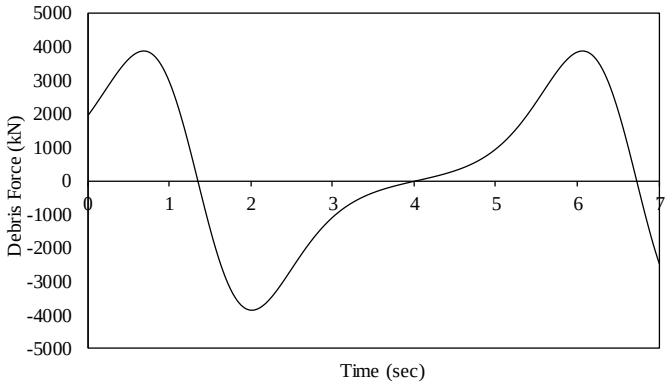


*Figure 3. Debris force time history*

## DAMAGE STATE DEFINITION

The damage states (DS) considered for the piers and bearings are presented in Table 3 where four stages of damage level are defined as slight, moderate, extensive and collapse, respectively. The material strain-based damage detection technique is used to define the DSs for the pier drifts [5] and those for the bearing shear deformation are taken based on seismic analysis of bridges [18].

*Table 3. Damage states adopted for vulnerability assessment*

| Component | Damage State | EDP | Limiting Values* | |
|---|---|---|---|---|
| | | | Scenario 1 | Scenario 2 |
| Pier | DS-1 | Drift | 0.91% | 2.34% |
| | DS-2 | | 1.48% | 3.61% |
| | DS-3 | | 5.34% | 6.53% |
| | DS-4 | | 8.78% | 9.93% |
| Elastomeric Bearing | DS-1 | Shear Deformation | 20% | |
| | DS-2 | | 100% | |
| | DS-3 | | 200% | |
| | DS-4 | | 300% | |

*Note: Further details on the derivation of the DSs can be found in [5]

## RESULTS AND DISCUSSION

### Variation in component demands

Figures 4 and 5 show the variation in the maximum responses from the piers and bearing components due to the three load cases from all 20 bridge models. It is observed that the component responses due to case 3, which includes the tsunami debris load, are the highest. On the other hand, component responses due to case 1 are higher than those for case 2. To elaborate, the maximum pier drifts of B1 in scenario 1 are 2.36% and 0.98% for case 1 and 2 loading, respectively. The maximum bearing deformations in B1 during the same scenario are 777.34mm and 25.84mm for case 1 and 2, respectively. Also, it can be noted that the component responses are higher in scenario 2 compared to scenario 1. The flow speed considered in case 1 is the highest and the corresponding $T_w$ is the lowest among the three. From the study by Rahman and Billah [5], it is noted that the wave load intensity increases as $T_w$ decreases and that the $T_w$ is the most dominating wave parameter. This observation falls in line with this study as the maximum pier drift and bearing deformation during case 1 are all higher than those observed in case 2 even though the $H_w$ in case 2 is greater than that in case 1. Although the flow speed and flow depth, thereby the corresponding $T_w$ and $H_w$, are the smallest in case 3, highest pier drift and bearing deformations are observed in case 3 due to the effect of the large water-borne debris load. From both Figures 4 and 5, it is observed that although the same loading case is being applied, the extent of component responses is different in each bridge model. This is due to the difference in material properties in the piers. For instance, the highest pier drift is shown by the B4 model (Figure 4) which has the highest reinforcing steel yield strength. Moreover, the B1 pier has the lowest yield strength and correspondingly shows the lowest drift among the rest analyzed. Interestingly, it is observed that even though there is no change in the elastomeric bearing properties, the shear deformation of bearings in each bridge model is different (Figure 5). This is because the deformation of piers does influence the behavior of bearings. As discussed earlier, the piers in each model have different material property and undergoes different drift levels under the same load case. Due to this, the piers have different stiffness so different level of forces are attracted to them which is ultimately transferred to the bearings. Since the piers are experiencing different levels of forces, bearings will also undergo different forces which causes different deformations in bearings under the same intensity measure.

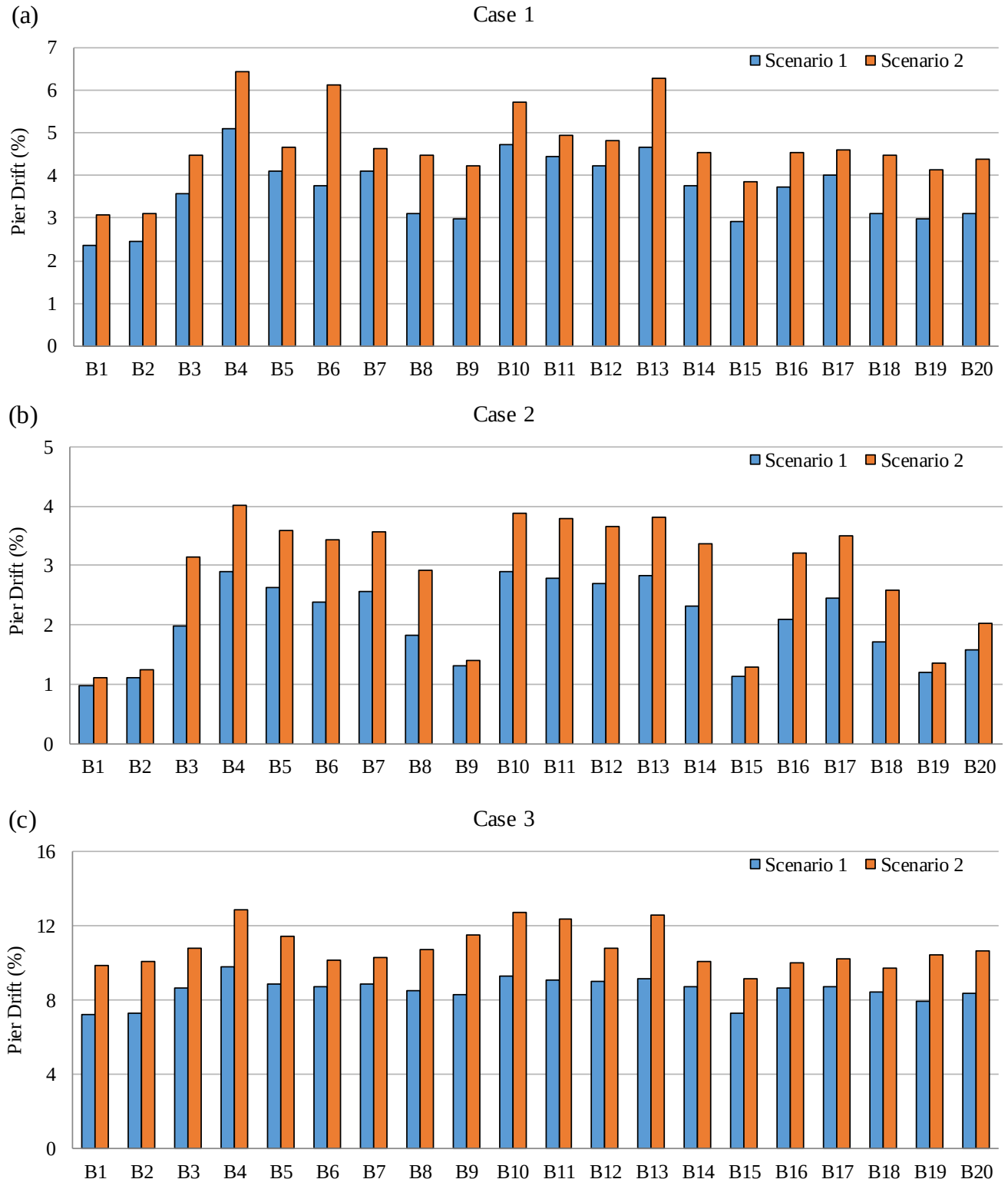


*Figure 4. Maximum pier drift recorded during scenarios 1 and 2 at (a) case 1, (b) case 2 and (c) case 3 tsunami loading*

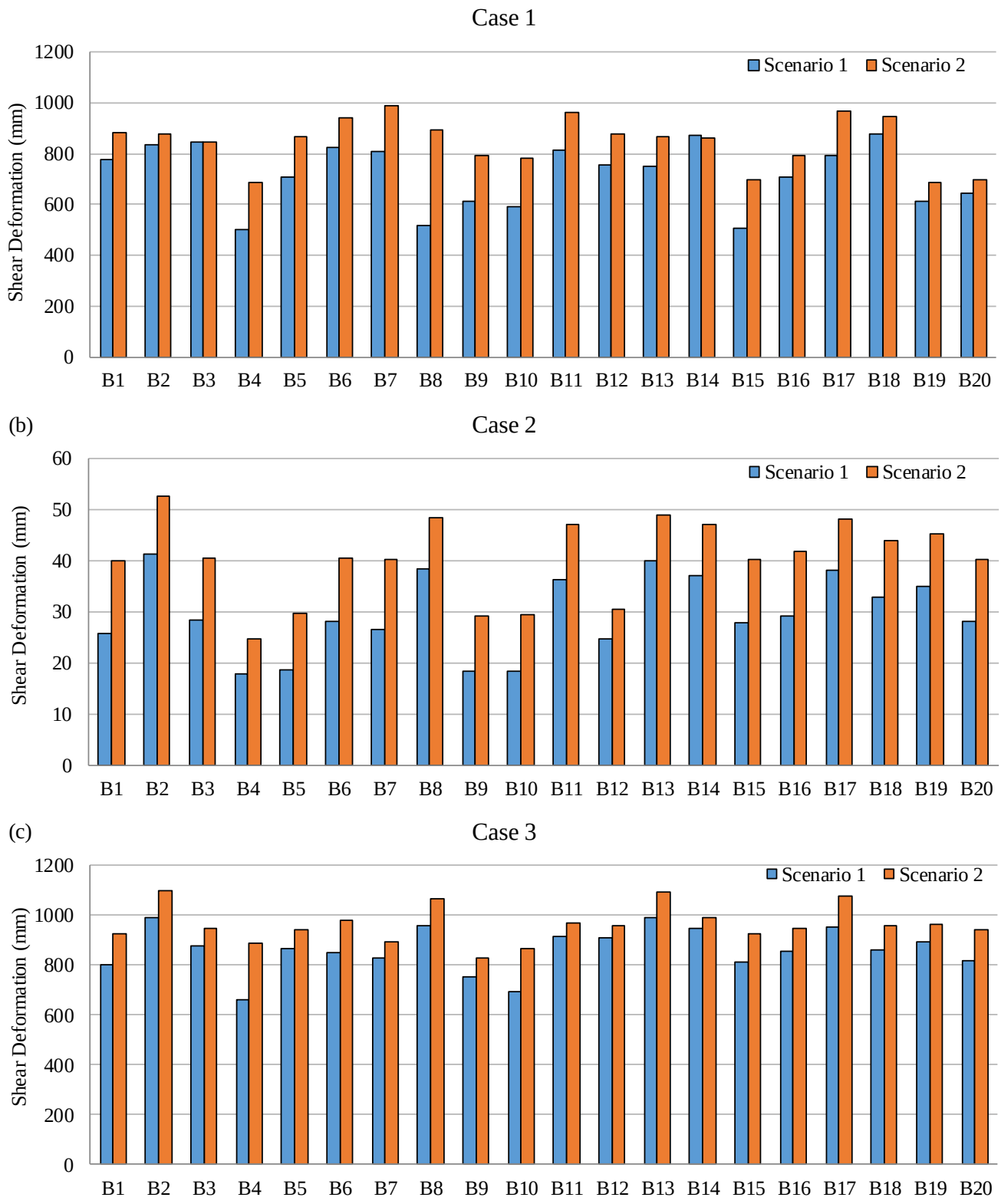


*Figure 5. Maximum shear deformation of the elastomeric bearing recorded during scenarios 1 and 2 at (a) case 1, (b) case 2 and (c) case 3 tsunami loading*

**Vulnerability assessment**

As part of the vulnerability assessment of this study, Figures 6 and 7 show the fraction of the maximum component responses exceeding the DSs as defined in Table 3 with respect to the $H_w$ and $T_w$ parameters considered. From Figure 6(a) it is observed that all the models exceeded DS-1 for all the load cases. However, the piers exceeded DS-2 but are within DS-3 at 4.67m wave height whereas 35% of the piers are found to collapse at a wave height of 3.15m. This is due to the fact that the lowest wave height is associated with the debris load case which causes the collapse of the piers. As the intensity of the wave load increases in scenario 2 (Figure 6(b)), 95% of the piers are found to exceed DS-4 at $H_w$ = 3.15m. Similarly, at the longest wave period of 5.06sec, the 35% of the piers are found to exceed the collapse state (DS-4) whereas, for the shortest wave period of 3.37sec, all the piers are within DS-3 although have exceeded DS-2 (Figure 6(c)). It is noted that 95% of the piers exceed DS-4 at $T_w$ = 5.06sec and 10% of the piers cross the extensive failure state (DS-3) in scenario 2 (Figure 6(d)) compared to scenario 1 where none of the piers exceeded DS-3 at $T_w$ = 3.37sec. From Figure 7, it can be observed that in all the cases, the elastomeric bearings exceed the collapse DS at case 1 and 3 tsunami loads irrespective of the difference in scenarios. However, the bearings are in the moderate damage zone (DS-2) for case 2 loading condition during both scenarios. For the same $H_w$ of 4.67m, none of the piers exceed DS-4, whereas the bearings in all the models are found to collapse. Upon comparing these results, it is evident that the bearing elements are the most vulnerable component.

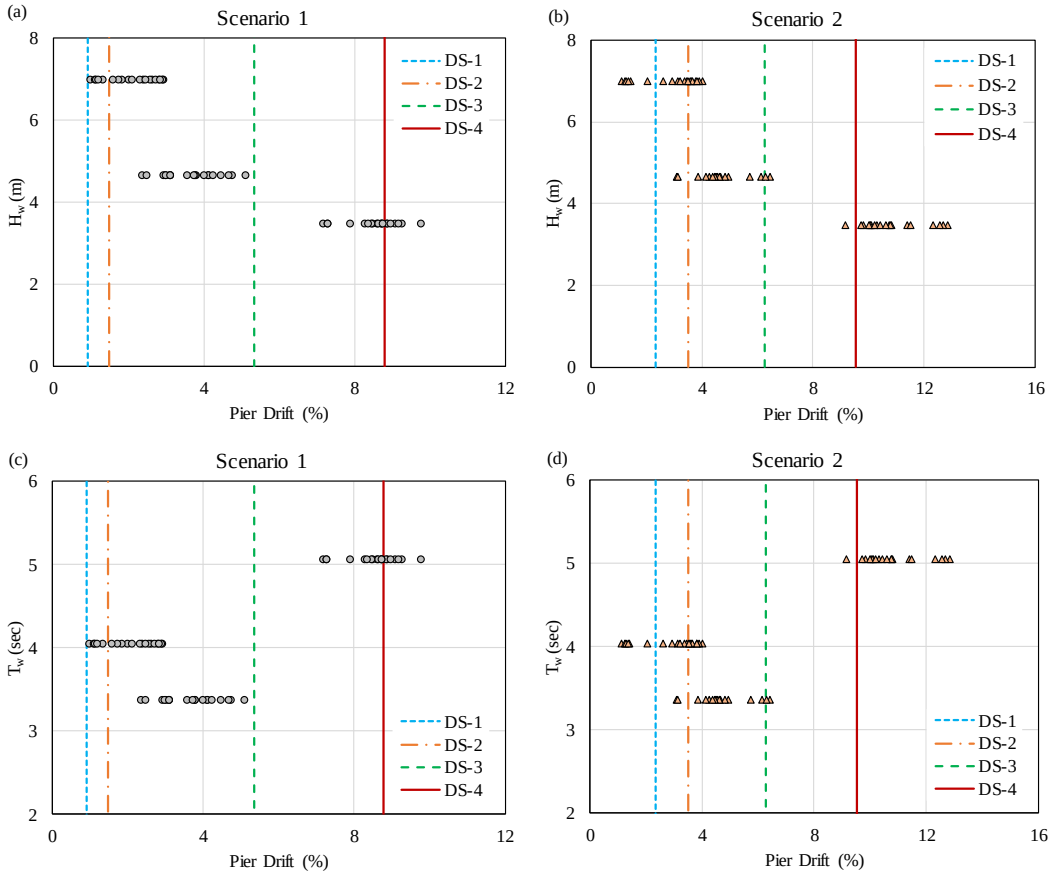


*Figure 6. Fraction of the maximum pier drift exceeding the DSs corresponding to (a) $H_w$ in scenario 1, (b) $H_w$ in scenario 2, (c) $T_w$ in scenario 1 and (d) $T_w$ in scenario 2.*

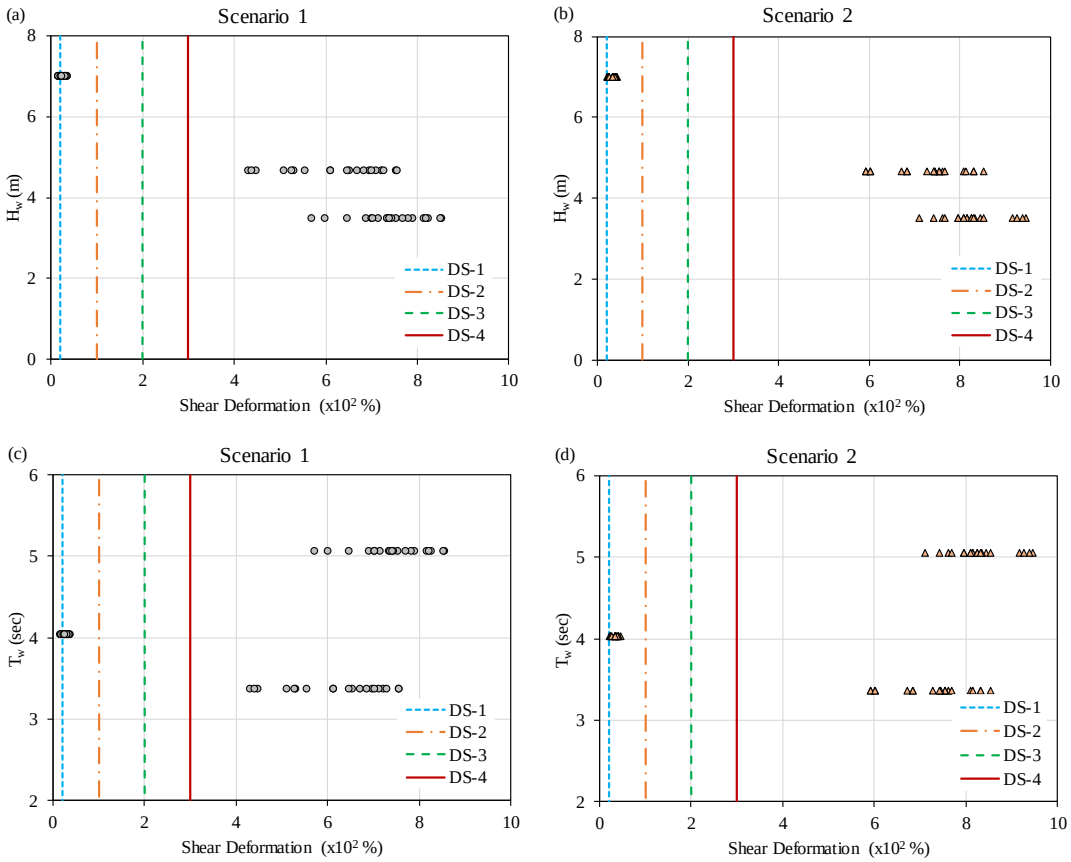


*Figure 7. Fraction of the maximum shear deformations by the elastomeric bearing exceeding the DSs corresponding to (a) $H_w$ in scenario 1, (b) $H_w$ in scenario 2, (c) $T_w$ in scenario 1 and (d) $T_w$ in scenario 2.*

## CONCLUSIONS

This study addressed the gap in vulnerability assessment of coastal bridges subjected to tsunami loads including debris flow. Three loading cases are chosen to represent the maximum flow speed with reduced flow depth, maximum flow depth with reduced flow speed and debris load with reduced flow speed and flow depth, respectively. Time history of the total vertical and horizontal tsunami loads are calculated using the wave period and wave height corresponding to the flow speed and depth of flow. A typical shipping container is assumed as the large water-borne debris load acting on the bridge models. This study analyzes both pier and deck level tsunami loading including the debris impact. Numerical analysis results representing the maximum responses from piers and bearing components are presented. Vulnerability assessment is carried out using the comparison of the maximum responses with the damage states developed earlier for a coastal bridge subjected to extreme wave-induced loads. The following conclusions can be drawn from the study.

1. The maximum pier drift and bearing deformations are observed due to case 3 tsunami loading even though the flow speed and depth were the least among the three cases highlighting the impact of debris load on the bridge system.
2. Component responses during case 1 (representing shortest wave period) loading are observed to be higher compared to that during case 2 (representing highest wave height) loading thereby confirming that wave period indeed has higher effect on the intensity of wave loads on the bridge.
3. For the same load case and scenario, the component responses are found to be different across all the bridge models. The pier drift ratios increased as the reinforcement yield strength increased and vice versa.
4. In general, both the piers and bearing components are more vulnerable in scenario 2 loading. The piers are found to exceed the moderate damage state but are within the extensive damage limit at a wave height of 4.67m in scenario 1. 35% of the piers in scenario 1 are found to exceed the collapse damage state at a wave height of 3.15m, which is increased to 95% in scenario 2.
5. The bearing deformation results remained within the moderate damage zone for the case 2 load representing a wave height and wave period of 7m and 4.04sec, respectively. However, all the bearing deformations are seen to exceed the

collapse damage state for both cases 1 and 3. This points out the fact that the bearings are more vulnerable than the piers during a tsunami.

## ACKNOWLEDGMENTS

This research was supported by the Natural Science and Engineering Research Council (NSERC) of Canada through the Discovery Grant and funding provided by University of Calgary through the start-up grant. This financial support is greatly appreciated.

## REFERENCES

[1] Goda, K., De Risi, R., De Luca, F., Muhammad, A., Yasuda, T., and Mori, N. (2021). "Multi-hazard earthquake-tsunami loss estimation of Kuroshio Town, Kochi Prefecture, Japan considering the Nankai-Tonankai megathrust rupture scenarios". *International Journal of Disaster Risk Reduction*, 54, 102050.

[2] Goda, K., Li, S., Mori, N., and Yasuda, T. (2015). "Probabilistic tsunami damage assessment considering stochastic source models: Application to the 2011 Tohoku earthquake". *Coastal Engineering Journal*, 57(03), 1550015.

[3] Azadbakht, M. and Yim, S.C. (2015). "Simulation and estimation of tsunami loads on bridge superstructures". *Journal of Waterway, Port, Coastal, and Ocean Engineering*, 141(2), 04014031.

[4] Feng, R., Zhu, D., and Dong, Y. (2022). "Dynamic performance of simply supported girder bridges subjected to successive earthquake-tsunami events". *Advances in Bridge Engineering*, 3(1), 10.

[5] Rahman, J. and Billah, A.M. (2023). "Development of Performance-Based Fragility Curves of Coastal Bridges Subjected to Extreme Wave-Induced Loads". *Journal of Bridge Engineering*, 28(3), 04023005.

[6] Qeshta, I. (2019). "Fragility and resilience of bridges subjected to extreme wave-induced forces", Ph.D. Thesis, RMIT University. Melbourne, Australia.

[7] Qeshta, I.M., Hashemi, M.J., Hashemi, M.R., Gravina, R.J., and Setunge, S. (2021). "Development of fragility functions for rigid-frame bridges subjected to tsunami-induced hydrodynamic forces". *Structure and Infrastructure Engineering*, 1-18.

[8] CSA S6:19 (2019). *Canadian Highway Bridge Design Code (CHBDC)*, CSA Group: Toronto, Ontario.

[9] Douglass, S.L. and Webb, B.M. (2020). *Highways in the Coastal Environment: Hydraulic Engineering Circular Number 25.* United States. Federal Highway Administration. Office of Bridges and Structures.

[10] Douglas, S.L., Chen, Q., Olsen, J.M., Edge, B.L., and Borwn, D. (2006). *Wave forces on bridge decks.* Final Report Prepared for U.S. Department of Transportation and Federal Highway Administration Office of Bridge Technology. Washington, D.C.

[11] McKenna, F., Fenves, G., and Scott, M. (2013). Computer program OpenSees: Open system for earthquake engineering simulation. Pacific Earthquake Engineering Center, University of California, Berkeley, CA. (http://opensees.berkeley.edu).

[12] Lynett, P., Thio, H.K., Scott, M., Murphy, T., Shantz, T., and Shen, J.-D. (2021). *Validation of Tsunami Design Guidelines for Coastal Bridges.* Report No. FHWA-OR-RD-21-09, Oregon. Department of Transportation Research Section and United States Department of Transportation. Washington, DC.

[13] NOAA (National Oceanic and Atmospheric Administration). National data buoy center. Accessed September 12, 2020. https://www.ndbc.noaa.gov/.

[14] Billah, A.H.M. and Alam, M.S. (2019). "Seismic fragility assessment of multi-span concrete highway bridges in British Columbia considering soil–structure interaction". *Canadian Journal of Civil Engineering*, 48(1), 39-51.

[15] Ataei, N., Stearns, M., and Padgett, J.E. (2010). "Response sensitivity for probabilistic damage assessment of coastal bridges under surge and wave loading". *Transportation research record*, 2202(1), 93-101.

[16] FEMA P-646 (2012). *Guidelines for design of structures for vertical evacuation from tsunamis*, 2nd Ed., Applied Technology Council: Washington, DC.

[17] Naito, C., Cercone, C., Riggs, H., and Cox, D. (2014). "Procedure for site assessment of the potential for tsunami debris impact". *Journal of Waterway, Port, Coastal, and Ocean Engineering*, 140(2), 223-232.

[18] Stefanidou, S.P. and Kappos, A.J. (2017). "Methodology for the development of bridge-specific fragility curves". *Earthquake Engineering & Structural Dynamics*, 46(1), 73-93.